Supplementary Information for 'Conforming nanoparticle sheets to surfaces with Gaussian curvature'

Noah P. Mitchell,[1,*] Remington L. Carey,[1,2] Jelani Hannah,[1] Yifan Wang,[1,3] Maria Cortes Ruiz,[1] Sean P. McBride,[1,4] Xiao-Min Lin,[5] and Heinrich M. Jaeger[1,†]

[1] *James Franck Institute and Department of Physics, University of Chicago, Chicago, IL 60637, USA*
[2] *Cavendish Laboratory, University of Cambridge, Cambridge, UK*
[3] *Division of Engineering and Applied Science, California Institute of Technology, Pasadena, CA, USA*
[4] *Department of Physics, Marshall University, Huntington, WV 25755, USA*
[5] *Center for Nanoscale Materials, Argonne National Laboratory, Argonne, Illinois 60439, USA*

BENDING

In Fig. 4 of the main text, we omit linear and sublinear dependences on the polar angle, θ, for clarity. As a result, the bending energies for different polar angles (blue, gray, and orange dashed lines) are shown to lie atop each other. Here we note that we expect some dependence of the bending energy density $\mathcal{E}_b$ on polar angle, though this should appear as a subleading, quadratic correction to the bending energy on the apex of a PS sphere. The leading behavior is therefore $E_b \sim (B/D)\,\delta r \sin\theta$, where B is the bending modulus of the sheet and D is the diameter of the sphere.

The two-dimensional bending energy density of a thin plate in plane stress is [1]

$$\mathcal{E}_b = \frac{B}{2}\left[\left(\nabla^2\zeta\right)^2 + 2(1-\nu)\left\{\left(\frac{\partial^2\zeta}{\partial x\partial y}\right)^2 - \frac{\partial^2\zeta}{\partial x^2}\frac{\partial^2\zeta}{\partial y^2}\right\}\right], \quad \text{(S1)}$$

where $\zeta(x,y)$ is the out-of-plane displacement of the plate and B is the bending modulus. Taylor expanding around $\theta = 0$, the energy density evaluates to

$$\mathcal{E}_b = \frac{4B}{D^2}\left[(\nu+1) + 2(\nu+1)\theta^2 + \frac{14\nu+17}{6}\theta^4 + \mathcal{O}\left(\theta^5\right)\right]. \quad \text{(S2)}$$

Thus, we expect the bending energy of a membrane to increase with polar angle. This analysis neglects the presence of neighboring spheres, which would further affect the θ dependence, particularly at large θ, where the small deflection assumption and the validity of Eqn. S2 breaks down.

STRETCHING

Definitions of stretching energy, strain, and stress

Assuming locally in-plane displacements $\mathbf{u}(r,\phi) = u_r(r,\phi)\hat{\mathbf{r}} + u_\phi(r,\phi)\hat{\boldsymbol{\phi}}$, we have strains [1]

$$\varepsilon_{rr} = \partial_r u_r \quad \text{(S3)}$$

$$\varepsilon_{\phi\phi} = \frac{1}{r}\partial_\phi u_\phi + \frac{1}{r}u_r \quad \text{(S4)}$$

$$\varepsilon_{r\phi} = \frac{1}{2}\left(\frac{1}{r}\partial_\phi u_r + \partial_r u_\phi\right). \quad \text{(S5)}$$

When the out-of-plane displacements are included, the expressions for strain become

$$\varepsilon_{rr} = \partial_r u_r + \frac{1}{2}(\partial_r\zeta)^2 \quad \text{(S6)}$$

$$\varepsilon_{\phi\phi} = \frac{1}{r}\partial_\phi u_\phi + \frac{1}{r}u_r + \frac{1}{2r^2}(\partial_\phi\zeta)^2 \quad \text{(S7)}$$

$$\varepsilon_{r\phi} = \frac{1}{2}\left(\frac{1}{r}\partial_\phi u_r + \partial_r u_\phi + \frac{1}{r}\partial_r\zeta\partial_\phi\zeta\right). \quad \text{(S8)}$$

These strains are related to the stress via

$$\sigma_{rr} = \frac{Y}{1-\nu^2}(\varepsilon_{rr} + \nu\varepsilon_{\phi\phi}) \quad \text{(S9)}$$

$$\sigma_{\phi\phi} = \frac{Y}{1-\nu^2}(\varepsilon_{\phi\phi} + \nu\varepsilon_{rr}) \quad \text{(S10)}$$

$$\sigma_{r\phi} = \frac{Y}{1+\nu}\varepsilon_{r\phi}, \quad \text{(S11)}$$

where $Y = Et$ is the stiffness.

The stretching energy density, $\mathcal{E}_s = \frac{1}{2}\sigma_{ij}\varepsilon_{ij}$, takes the plane stress form

$$\mathcal{E}_s = \frac{Y}{1-\nu^2}\left(\frac{\varepsilon_{rr}^2 + \varepsilon_{\phi\phi}^2}{2} + \nu\varepsilon_{rr}\varepsilon_{\phi\phi}\right) + \frac{2Y}{1+\nu}\varepsilon_{r\phi}^2. \quad \text{(S12)}$$

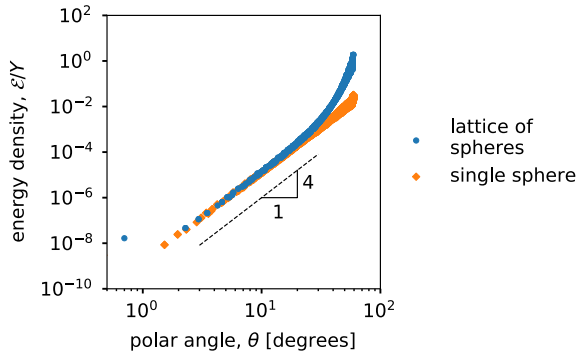

FIG. S1. **Stretching energy in a spring network draped on a lattice of spheres with strong pinning.** The energy density in a pinned sheet draped to a lattice of spheres grows as θ^4. Only at moderately large polar angles ($\theta \gtrsim 25^\circ$) does the stretching energy in a sheet conforming to a triangular lattice of spheres (blue circles) diverge from the case of a single sphere (orange diamonds). The quartic scaling with polar angle is exact in the absence of neighboring substrate spheres (orange diamonds). Both spring networks were $100\,a \times 100\,a$ in extent, and the substrate sphere diameters were $40\,a$ and $60\,a$ for the lattice and single sphere cases, respectively.

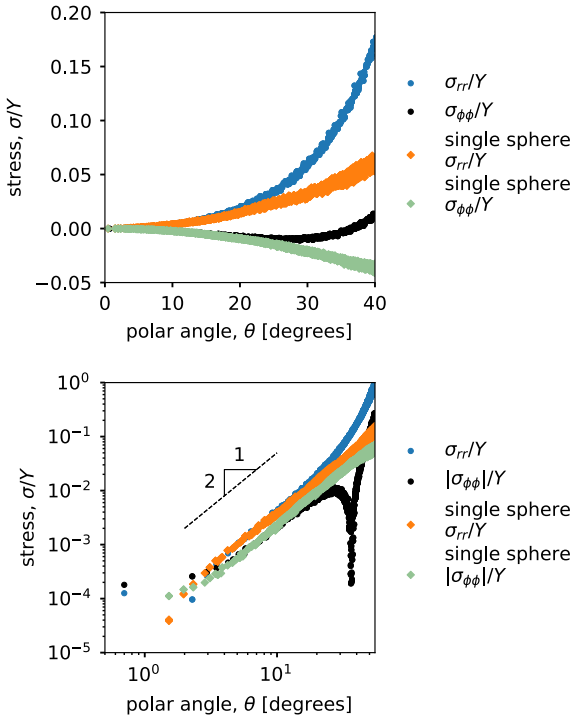

FIG. S2. **In-plane stresses in a spring network draped on a lattice of spheres with strong pinning.** The stress density in a pinned sheet draped to a lattice of spheres grows as θ^2. Only at moderately large polar angles ($\theta \gtrsim 25^\circ$) does the stretching energy in a sheet conforming to a triangular lattice of spheres (blue circles) diverge from the case of a single sphere (orange diamonds). The quadratic scaling with polar angle is exact in the absence of neighboring substrate spheres (gray and orange diamonds for σ_{rr} and $\sigma_{\phi\phi}$, respectively.) The lattice dimensions are the same as in Fig. S1.

Since $\varepsilon_{r\phi} = 0$ by symmetry on the sphere,

$$\mathcal{E}_s = \frac{Y}{1-\nu^2}\left(\frac{\varepsilon_{rr}^2 + \varepsilon_{\phi\phi}^2}{2} + \nu\varepsilon_{rr}\varepsilon_{\phi\phi}\right). \qquad \text{(S13)}$$

Sequential pinning gives $\mathcal{E}_s \sim Y\theta^4$

Fig. S1 shows the stretching energy of an elastic spring network as a function of polar angle on the sphere. We find the stretching energy density grows as $\mathcal{E}_s \sim Y\theta^4$ for modest polar angle. Additionally, each component of the stress exhibits $\sigma \sim Y\theta^2$ scaling, particularly when only a single sphere is present as the substrate, as shown in Fig. S2. The presence of neighboring spheres in the substrate causes deviation from the power-law scaling in both energy density and stress for sufficiently large polar angles ($\theta \gtrsim 25^\circ$). The quadratic scaling of the strain, ε, can likewise be seen in Fig. 6 of the main text.

The geometric frustration of the sheet on the spherical cap is the source of elastic energy in an annulus of the sheet that has not yet conformed to the sphere. In particular, let us consider the portion of the sheet near θ_a which is just about to adhere to the sphere, and is therefore about to become pinned in its current state of strain. The strain at θ_a scales linearly with the integrated Gaussian curvature of the spherical cap: $\varepsilon \sim \int_0^{R\theta_a} G\, r\, \mathrm{d}r \sim \int_0^{R\theta_a} (1/R^2)\, r\, \mathrm{d}r \sim R^0\theta_a^2$, where $R = D/2$ is the radius of the sphere [2, 3]. This portion of the sheet is then frozen into a strain configuration that depends quadratically on the polar angle at which it conforms. As a result, after many annuli have adhered, each corresponding to a ever-larger θ_a, we expect $\varepsilon \sim \theta^2$. Linear elasticity dictates that the stress scales similarly as well — $\sigma \sim Y\varepsilon \sim Y\theta^2$, where Y is the stiffness — and thus the stretching energy density $\mathcal{E}_s = \frac{1}{2}\sigma\varepsilon \sim Y\theta^4$. This means that the stretching energy stored in an annulus is $E_s \sim YD\,\delta r\,\theta^4 \sin\theta$, which for small θ gives $E_s \sim YD\,\delta r\,\theta^5$. Sequential pinning of the nanoparticle sheet ensures that

this is true irrespective of the maximum angle subtended by the sheet: the state of strain is frozen into the adhered portion, unable to respond elastically to additional pileup of strain at $\theta > \theta_a$.

Case without pinning has different $\mathcal{E}_s$ scaling

This analysis contrasts with the expectation for an equilibrated elastic sheet without pinning. Without pinning, the energy density rearranges in such a way as to be non-monotonic in the polar angle θ on the sphere, with some sensitivity to the boundary conditions. The stress is greatest on the apex of a sphere without pinning, in stark contrast to the case with sequential pinning, for which the stress vanishes at the cap. This difference highlights the distinct character of sequential adhesion to a substrate seen in our system.

Without pinning, we can solve for the strain energy by finding the stress and strain via

$$\frac{1}{Y}\nabla^4\chi(r) = -G = -\frac{1}{R^2}, \tag{S14}$$

where χ is the Airy stress function given by $\sigma_{ij} = \varepsilon_{il}\varepsilon_{jk}\partial_l\partial_k\chi$ and where, as before, $R = D/2$ is the radius of the sphere. Solving Eqn. S14 for the energy density in a circular sheet of radius W equilibrated to a spherical cap results in

$$\begin{aligned}\mathcal{E}_s(r) =& \frac{G^2Y}{256}\left[(5-3\nu)r^4 - 4(1-\nu)r^2W^2\right.\\ &\left.+(1-\nu)W^4\right]\\ &+\frac{GP(\nu-1)}{8Y}\left(2r^2-W^2\right)+\frac{T^2(1-\nu)}{Y},\end{aligned} \tag{S15}$$

where r is the radial coordinate of the polar coordinate system on the apex of the sphere, and the apex is assumed to coincide with the center of the circular sheet. Here, $T = \sigma_{rr}(r = W)$ is the radial stress at the boundary. If we set $T = 0$ for the moment to look only at the effects of curvature, for small polar angles $\theta \approx r\sqrt{G}$, the energy density *decreases* with polar angle in a quadratic correction:

$$\mathcal{E}_s \approx \frac{G^2Y(1-\nu)}{256}\left[W^4 - \frac{4W^2}{G}\theta^2 + \mathcal{O}(\theta^4)\right]. \tag{S16}$$

If we set $W = R\theta_{\max} = D\theta_{\max}/2$, with $\theta_{\max}$ fixed, the leading term shows that $\mathcal{E}_s \sim YD^0\theta^0$. This behavior contrasts with the case with pinning studied elsewhere in this article. We note, however, that the *total* stretching energy in the entirety of a spherical cap conformed to a sphere, with or without pinning, has the *same* scaling: $E_s^{\text{tot}} \sim YD^2\theta_{\max}^6$, where $\theta_{\max}$ is the maximum angle at the edge of the sheet.

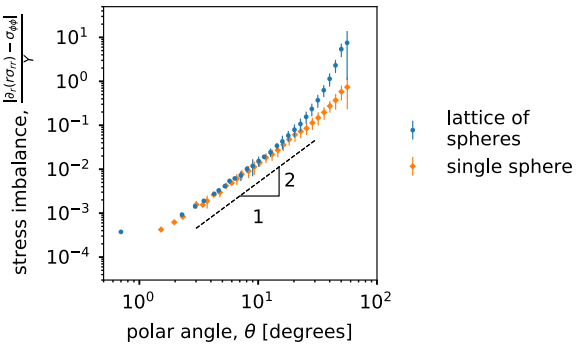

FIG. S3. **Adhesion enables an in-plane stress imbalance to the elastic membrane.** Through adhesion to the substrate, there is a residual force imbalance in the stretching of a simulated triangular spring network. The quadratic scaling with polar angle is exact in the absence of neighboring substrate spheres (orange diamonds). Both spring networks were $100\,a \times 100\,a$ in extent, and the substrate sphere diameters were $40\,a$ and $60\,a$ for the lattice and single sphere cases, respectively.

Influence of adhesion

Fig. S3 shows that for modest polar angles, the in-plane stress imbalance

$$\mathcal{I} \equiv \partial_r\left(r\sigma_{rr}\right) - \sigma_{\phi\phi} \tag{S17}$$

grows quadratically in simulations of spring networks draping to spheres. Without adhesion, this quantity would vanish in equilibrium. We checked that the residual force imbalance is scale-independent for sufficiently large substrate sphere sizes ($D/a \gtrsim 10$).

Case without pinning does not agree with experiment

If adhesion is not included, then the resulting strain field contrasts with the results from simulations, as shown in Fig. S4. The strain fields in this

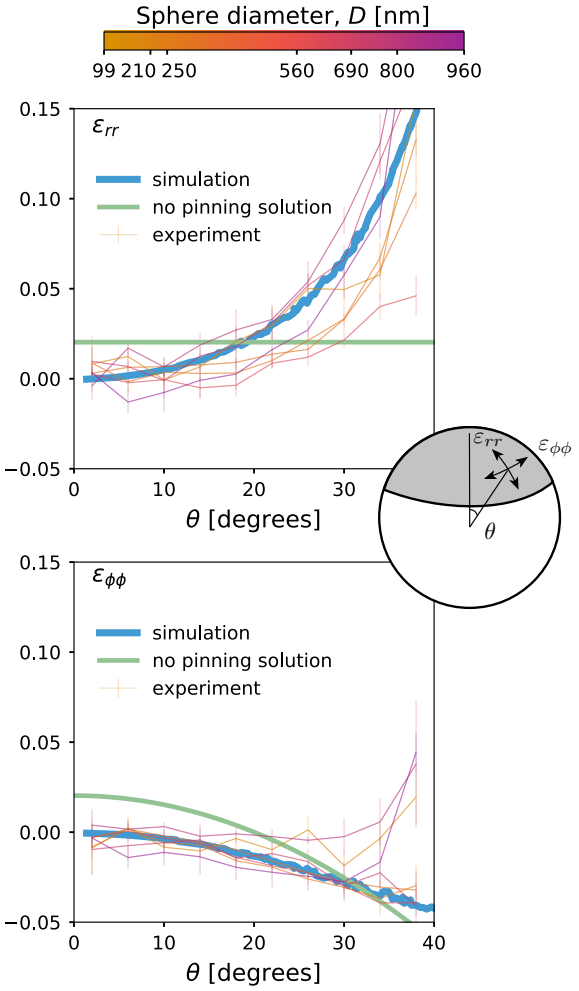

FIG. S4. **Strong pinning to the substrate is necessary for qualitative agreement with experiments.** The analytic solution in the case with no adhesion, given by the green curve, differs qualitatively from the simulation (blue curve) and experimental results (transparent orange and purple data).

case are

$$\varepsilon_{rr} = \frac{1}{16}\left[(3\nu-1)\theta^2 + 4(1-\nu)\frac{W^2}{D^2}\right] \qquad \text{(S18)}$$

$$\varepsilon_{\phi\phi} = \frac{1}{16}\left[(\nu-3)\theta^2 + 4(1-\nu)\frac{W^2}{D^2}\right], \qquad \text{(S19)}$$

where W is the width of the sheet from the cap to the periphery. We assume the radial stress vanishes at the boundary for simplicity ($T = 0$), but we note that changing T simply adds a constant to each strain component. In Fig. S4, W was taken to be the radius of the sphere, $D/2$, times 40° — approximately where cracks appear in Fig. 2c of the main text. The qualitative differences in elastic response shown in Fig. S4 highlight the importance of adhesion in determining the mechanical response and monolayer morphology.

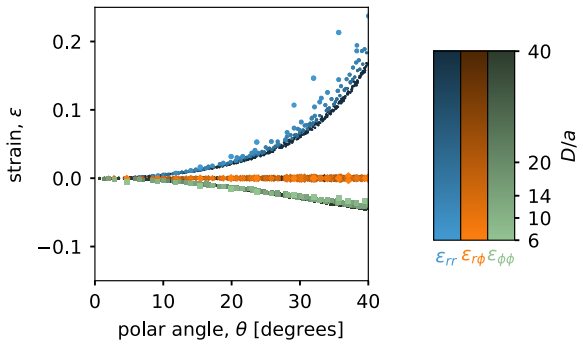

FIG. S5. **Finite size effects in the energetics of draped spring networks.** Spring networks with lattice spacing a were draped over seven spheres in a triangular closed packed arrangement, as in Fig. 1 of the main text. The resulting strains depend only weakly on the ratio of sphere size to lattice spacing, D/a, so that the data coincide for all but the smallest values of D/a. While the shear and azimuthal strains are nearly unaffected by the size of the lattice, the radial strain begins to diverge significantly around $D/a \sim 10$.

Finite size effects in draped spring networks

We investigated the effects of finite size in the simulations of spring networks with respect to the substrate sphere size. Spring networks with lattice spacing a are draped over seven spheres in a triangular closed packed arrangement, as in Fig. 1 of the main text. The resulting strains depend weakly on the ratio of sphere size to lattice spacing, D/a. While the shear and azimuthal strains are nearly unaffected by the size of the lattice down to values of $D/a \sim 6$, the radial strain begins to diverge significantly around $D/a \sim 10$. This is reminiscent of previous work on nanoparticle membranes [4], where the influence of the discrete lattice becomes significant for systems with a characteristic size of $\sim 10\,a$.

Sensitivity to conformation geometry

In simulations reported so far, we have used a sheet geometry in which each nanoparticle lies ei-

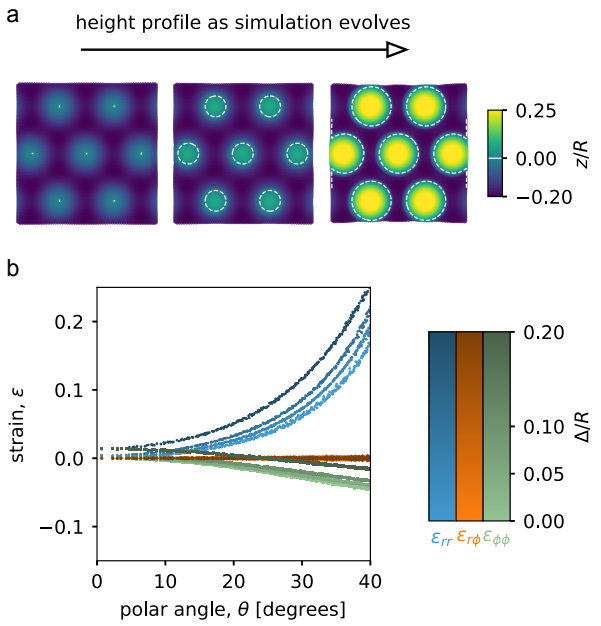

FIG. S6. **Introducing a model indentation that penetrates the interstices of the lattice of substrate spheres changes the resulting nanoparticle sheet strain fields only slightly.** *(a)* The spring network relaxes on a corrugated surface, which is lowered onto a lattice of seven spheres. The white dashed curves mark the $z = 0$ point, which is identified with the maximum height of the corrugated surface, $V(\mathbf{x})$, in the absence of substrate spheres. The spheres then protrude from this surface as the simulation evolves, and the spring network relaxes on a surface $z = \max\{V(\mathbf{x}), z_{\text{spheres}}\}$. Here the corrugation has a maximum depth of $\Delta = 0.2R$, where R is the radius of each substrate sphere. *(b)* Changing the indentation depth results in only modest changes in the strain configuration of the pinned sheet at the end of the simulation. Each value of maximum indentation depth, Δ, corresponds to each shade of blue (ε_{rr}), orange ($\varepsilon_{r\phi}$), and green ($\varepsilon_{\phi\phi}$) curves. As Δ (here normalized by the substrate sphere radius R) increases from simulation to simulation, the qualitative behavior of the strains remains relatively unchanged.

ther in an xy plane at a decreasing z position or on a sphere, whichever has a greater value of z coordinate. However, we do not expect that the nanoparticle sheet will be truly flat in the interstices of the PS spheres in our experiments. For the simulations presented earlier, the sheet is equilibrated in each timestep on a surface defined by $z = \max\{z_{\text{plane}}, z_{\text{spheres}}\}$ — that is, each node of the network may reside on either a substrate sphere or in a plane which is lowered incrementally at each time step. At the end of each time step, nodes that reside on a substrate sphere are pinned to that location permanently.

Fig. S6 shows that introducing a model indentation between substrate spheres elevates the observed strains of the final, pinned nanoparticle sheet. In Fig. S6b, each set of curves for ε_{rr}, $\varepsilon_{r\phi}$, and $\varepsilon_{\phi\phi}$ corresponds to a new simulation in which the spring network is iteratively stamped onto a lattice of spheres while conformed not to a plane, but to a corrugated surface with indentations penetrating the interstices of the substrate spheres (Fig. S6b). The networks are relaxed on a surface defined by $z = \max\{V(\mathbf{x}), z_{\text{spheres}}\}$, where

$$V(\mathbf{x}) = \Delta\big(\cos(\mathbf{b}_1 \cdot \mathbf{x}) + \cos(\mathbf{b}_2 \cdot \mathbf{x}) + \cos\left[(\mathbf{b}_1 + \mathbf{b}_2) \cdot \mathbf{x}\right]\big), \quad \text{(S20)}$$

where $\mathbf{b}_1$ and $\mathbf{b}_2$ are the reciprocal lattice vectors of the honeycomb lattice defined by the position of the interstices. This corrugated surface changes the angle of contact between the spring lattice and the substrate spheres and acts as a source of strain in the interstices. While the qualitative strain behavior of the resulting pinned spring lattices remains largely unaltered, the radial and azimuthal strains grow with indentation depth, Δ. Future work could implement a more realistic boundary condition for downward pressure on the sheet, as $V(\mathbf{x})$ is a highly simplified surface.

OTHER POSSIBLE SCALING DIAGRAMS

In section 3 (entitled 'Energy Scaling') and Fig. 4 of the main text, we presented a competition of energy scales that captures the observed behavior of our nanoparticle sheets. Here we note that, in a different material, the energetic cost of plastic deformation, captured via the phenomenological factor Γ, could be much larger than the adhesion energy, γ, then the plastic deformation regime might be absent, since no crossover between E_γ and E_d would occur. This situation is illustrated in Fig. S7.

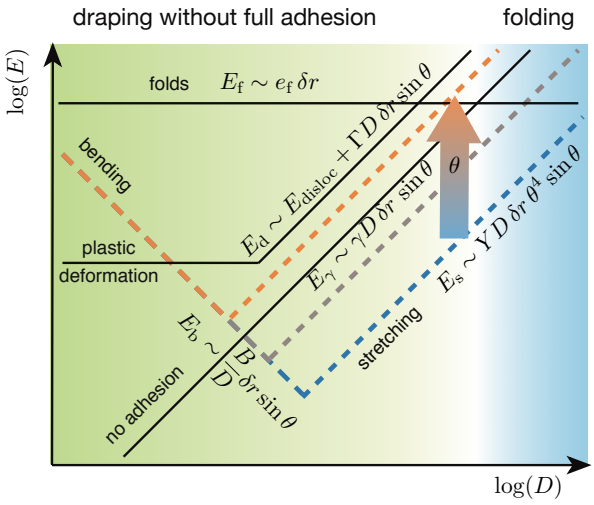

FIG. S7. **A nanoparticle sheet's material properties could be altered such that $E_d > E_\gamma$ for all sphere sizes D.** For this ordering of competing energy scales, there is only a transition from incomplete adhesion at small sphere sizes to folding at large sphere sizes.

* npmitchell@uchicago.edu; Corresponding author
† jaeger@uchicago.edu; Corresponding author

[1] L. D. Landau and E. M. Lifshitz, in *Theory of Elasticity (Third Edition)* (Butterworth-Heinemann, Oxford, 1986) pp. 38–86.
[2] N. P. Mitchell, V. Koning, V. Vitelli, and W. T. M. Irvine, Nature Materials **16**, 89 (2017).
[3] V. Vitelli, J. B. Lucks, and D. R. Nelson, Proceedings of the National Academy of Sciences **103**, 12323 (2006).
[4] Y. Wang, J. Liao, S. P. McBride, E. Efrati, X.-M. Lin, and H. M. Jaeger, Nano Letters **15**, 6732 (2015).